Supplement to: Development of Volatility Distributions of Biomass Burning Organic Emissions

Aditya Sinha[1], Ingrid George[2], Amara Holder[2], William Preston[3], Michael Hays[2], Andrew Grieshop[1]

[1]Department of Civil and Environmental Engineering, North Carolina State University, Raleigh, NC

[2]Center for Environmental Measurement and Modeling, Environmental Protection Agency, Durham, NC

[3]CSS Inc., Durham, NC

Data underlying all figures in manuscript and supplement can be freely access at : doi:10.5061/dryad.jsxksn0ct

Section S1: Comparison of aerosol mass in particle phase from partitioned TD/GC/MS and artifact corrected filter measurements

To ensure consistency in our measurement approaches, we compare organic aerosol in the particle phase as measured by collection on quartz filters against organic aerosol observed in TD/GC/MS filter-in-tube chromatograms, after accounting for partitioning.

Combustion emissions were sampled onto bare quartz (BQ) filters and analyzed using thermo-optical methods to quantify organic carbon content. Primary organic carbon (OC) was estimated for positive artifact due to vapor absorption using a quartz-behind teflon (QBT) filter method.1 The artifact-corrected OC is calculated as the difference between the OC concentration on a front quartz filter and the OC concentration on a parallel quartz filter positioned behind a teflon filter. Note that the QBT filters were not collected for field samples and so estimates from BQ filters were used directly. The artifact percentage (QBT/BQ $\times$ 100) is less than 1% for burnhut, 17% for RWC-Startup and 14% for RWC-high fire. The OC concentrations were also background corrected using measurements taken from background filter samples collected at the test sites. To estimate primary organic aerosol concentrations (POA) we applied a campaign average estimate of the OM/OC ratio of 1.53 to the calculated OC mass concentrations. In the second method, we use the volatility distributions derived from TD/GC/MS chromatograms from filter-in-tube sorbent samples (described in section 2.3) to estimate POA in the particle phase. For each experiment, we use the partitioning equation (equation 1 in manuscript) at the POA concentration measured by the quartz filter, to calculate the particle fraction (X_p) in each volatility bin for the basis set of saturation concentration: $[10^{-2},10^{-1},10^{0},10^{1},10^{2},10^{3},10^{4},10^{5},10^{6}]$ μg m^{-3}. We then calculate the mass in the particle phase in each bin by using the total organic mass (particle + gas) in a volatility bin as measured by the filter-in-tube chromatograms and the particle fraction, X_p. Figure S9 shows the particle phase masses summed up and presented as an emission factor.

Comparing these two methods showed that EFs derived using the filter-in-sorbent tube method were biased low relative to filter-derived derived POA EFs. The divergence was largest for open field burns (burn-average correction factor of 10.36 – reflecting an order of magnitude divergence) and smallest for residential woodstove emissions (test average correction factor of 2.82). Several issues may contribute to the under-estimation of the TD/GC/MS mass. For example, it is possible that some organic material does not elute from the chromatogram but is measured on filter samples or perhaps the difference in mass is due to the uncertainty in response in the TIC analyzed using the *n*-alkane based calibration resulting in the observed disparity. To reconcile this difference, an averaged correction factor was calculated using the ratios of POA EFs from the two methods across the replicate samples of each combustion source. The bin masses estimated from the TD/GC/MS method are then corrected using these factors. To make this correction we assume that the impact of the divergence between the two methods is evenly distributed across the volatility bins. This assumption cannot be directly tested and is thus a source of uncertainty.

The averaged correction factors applied for each combustion source type are shown in Figure S9.

Table S1: Operating parameters of the TD/GC/MS system – Gerstel and Cooled Injection System inlet conditions, GC oven conditions and MS conditions.

Gerstel and CIS inlet conditions	
Gerstel Temperature ("C) ramp	25°C ramped to 300° at 60°C/sec hold 7 min
Inlet type	PTV
CIS cold trapping temperature	-100°C
Mode	Solvent Vent
Carrier gas	He
Purge flow to split vent (mL/min)	50
Column	30 m * .25 mm id HP 5 MS Ul
Column flow rate (ml/min)	1
GC oven conditions	
Initial oven temperature ("C)	65
Initial oven hold time (min)	10
Oven temperature ramp rate ("C/min)	10
Final oven temperature ("C)	300
Final oven hold time (min)	26.5
Maximum column temperature ("C)	325
MS conditions	
solvent delay time (min)	5.5
GC/MS interface temperature ("C)	300
data collection mode	Scan
scan range (amu)	50-500
MS source temperature ("C)	230
MS quad temperature ("C)	150

Table S2: Components of calibration compounds spiked on Carbotrap C/ Carbotrap F adsorbent tubes along with solvent (HIB solution) and internal standard. Spikes were prepared of 10 ng of each component for the sets of standard mixture.

S.No.	Type of Standard	Components	Molecular Weight (g/mol)
1	Alkane Standard	C10 – C38 (all even)	142.3 – 535.0
2	PAH Standard	Acenaphthylene	152.2
		Anthracene	178.2
		Benz[a]anthracene	228.3
		Benzo[b]fluoranthene	252.3
		Benzo[k]fluoranthene	252.3
		Benzo[ghi]perylene	276.3
		Benzo[a]pyrene	252.3
		Chrysene	228.3
		Dibenz[a,h]anthracene	278.4
		Fluorene	166.2
		Indeno[1,2,3-cd]pyrene	276.3
		Phenanthrene	178.2
		Pyrene	202.3
3	Methoxy Phenol Mix	Syringol	154.2
		Guaicol	124.1
		p-Cresol	108.1
		o-Cresol	108.1
		m-Cresol	108.1
		Vanillin	152.1
4	TCLP Acid Mix	2-Methylphenol (o-cresol)	108.1
		3-Methylphenol (m-cresol)	108.1
		4-Methylphenol (p-cresol)	108.1
		Pentachlorophenol	266.3
		2,4,5-Trichlorophenol	197.4
		2,4,6-Trichlorophenol	197.4
5	Phenol	Phenol	94.1
6	BB Sugar Mix	Levoglucosan	162.4

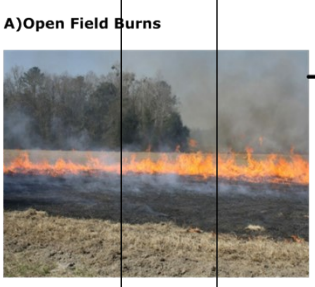

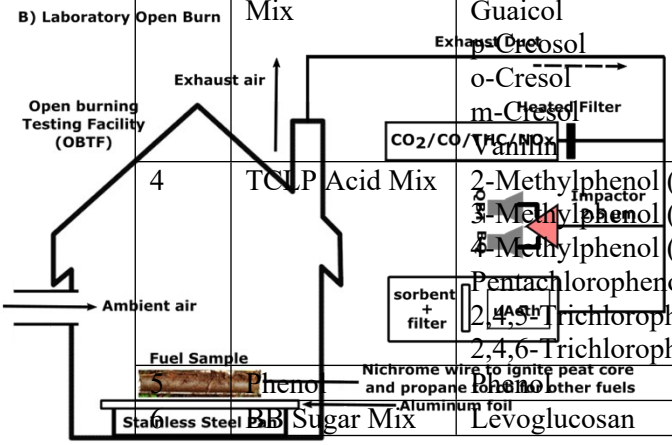

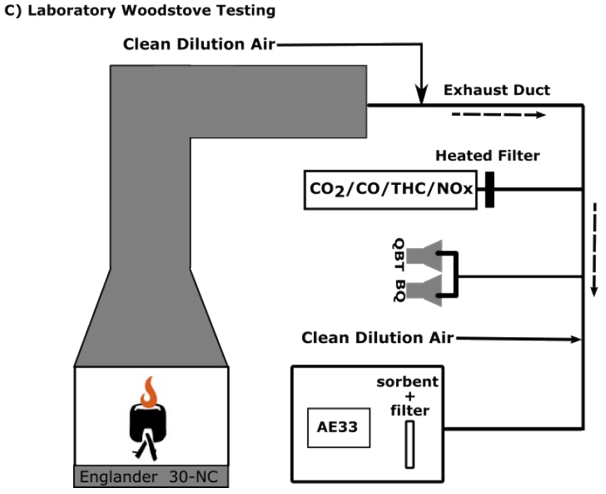

Figure S1: A) Experimental schematic for collection of emissions from open field burning. The measurement package was placed downstream of the burning field and included gas and particle phase measurements. B) Experimental schematic for collection of emissions from laboratory simulated open burning. Testing was carried out in the open burning testing facility (OBTF)[1] C) Experimental schematic for collection of emissions from laboratory woodstove testing.

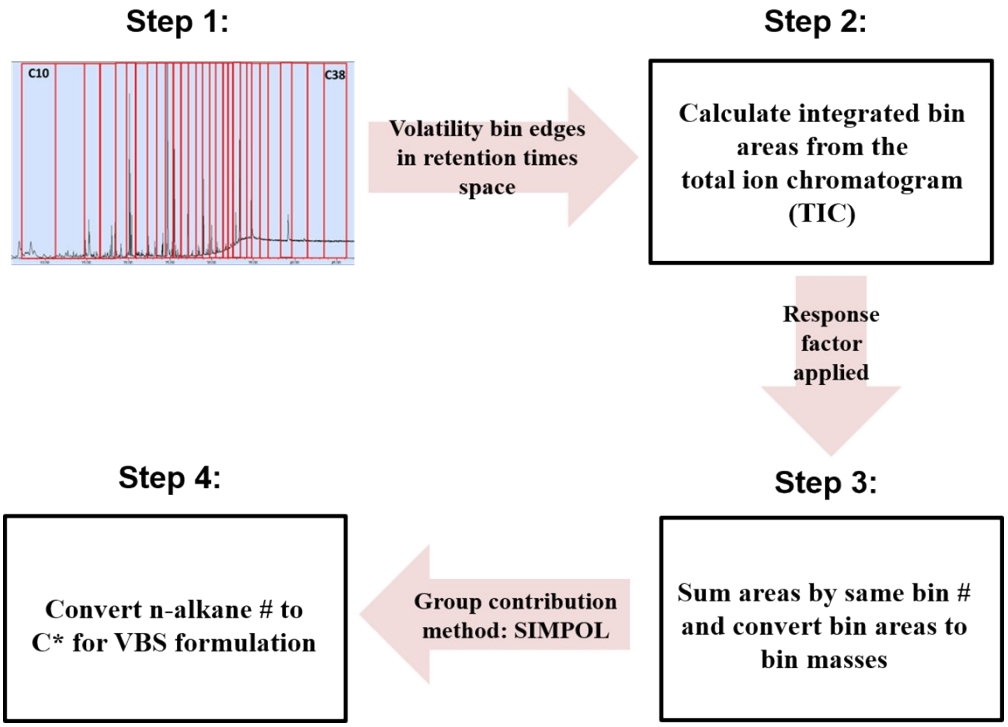

Figure S2: Flow chart depicting the various steps involved in the transformation of the raw total ion chromatogram (TIC) to depictions of volatility distribution using the volatility basis set (VBS) framework.

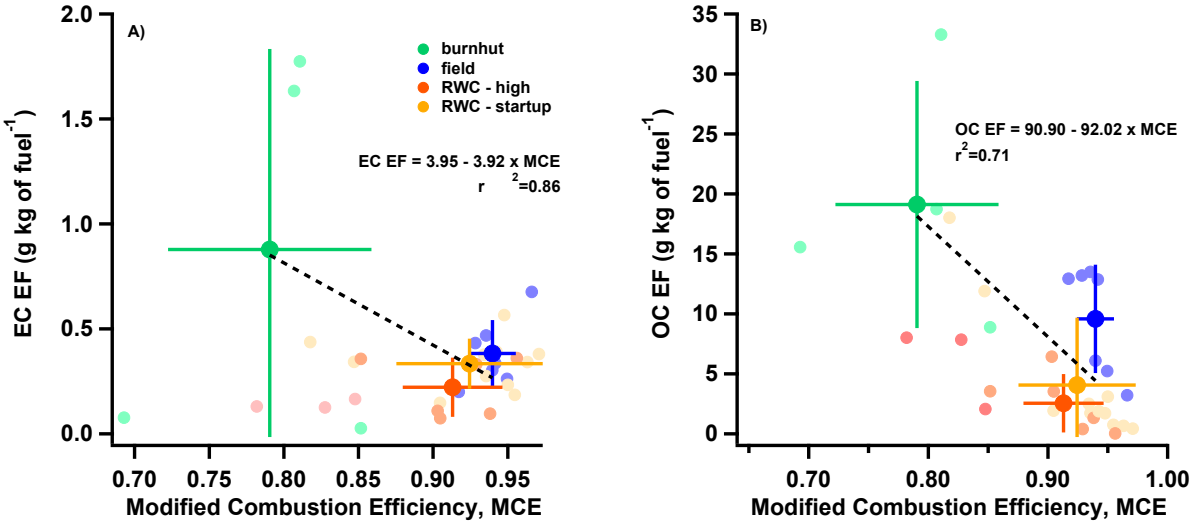

Figure S3: A) Elemental carbon emission factors (EC EFs) and B) Organic carbon emission factors (OC EF) as function of modified combustion efficiency (MCE) for different source emissions – burnhut, field, RWC phases (delineated by color). Faded markers represent test-averaged observations from integrated filter measurements while darker markers show the average $PM_{2.5}$ EF and MCE from a source emissions type with the error bars denoting the standard deviation across individual tests.

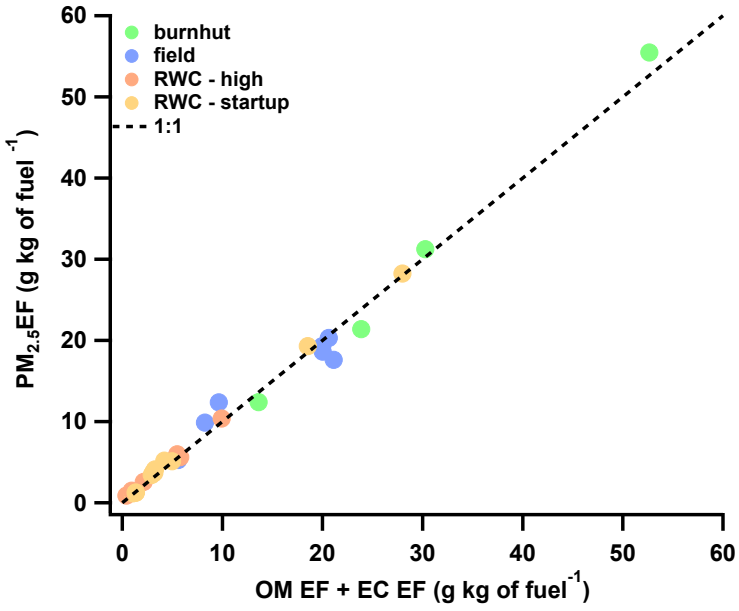

Figure S4: $PM_{2.5}$ emission factors, $PM_{2.5}$ EF (from gravimetric filter measurements) plotted against OM EF + EC EF (thermo-optical filter measurements). OC EFs are converted to OM EFs using an OM/OC ratio of 1.53, the average for all samples calculated assuming OM + EC = $PM_{2.5}$ in all cases (a simplification). Combustion sources are delineated by color. The dashed black line shows the 1:1 line

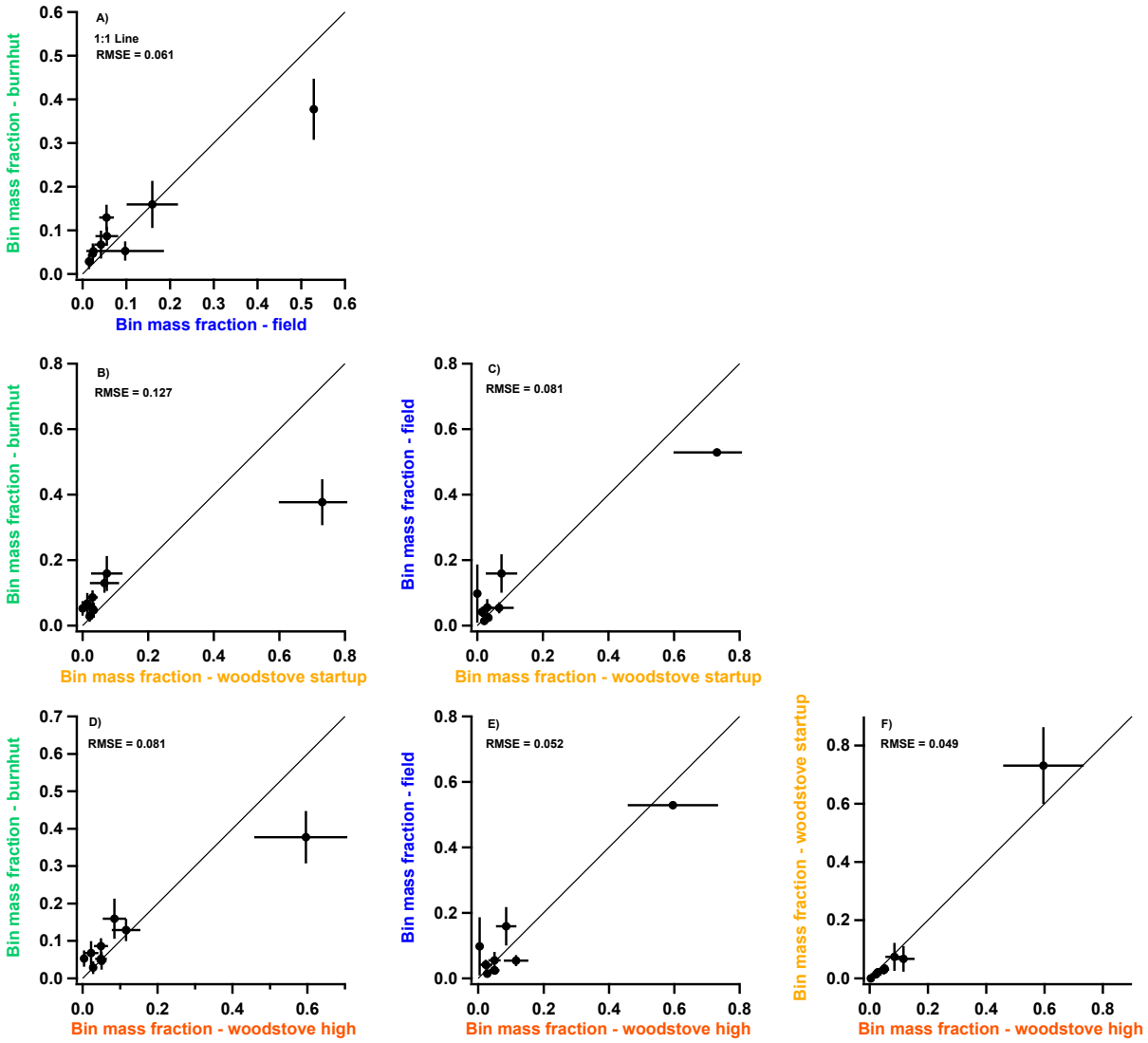

Figure S5: Scatter plots of the bin mass fraction contributions from volatility distributions in the range $-2 \leq logC^{*} \leq 6$ derived from TD/GC/MS chromatograms. The plots presented here include all combinations of comparisons between burnhut, field, RWC – high and RWC – startup distributions (delineated by label colors). The markers represent the average bin mass fraction from replicate (N=3) filter-in-tube samples while the error bars show the standard deviations in the replicates. The solid black line shows the 1:1 line in each plot with the root mean square error (RMSE) to the 1:1 line printed in each plot.

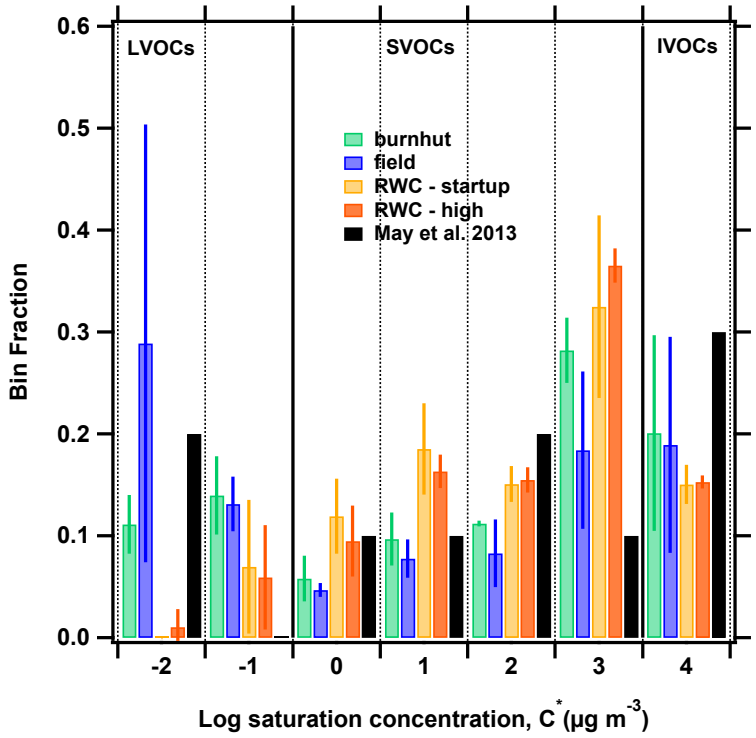

Figure S6: Volatility distributions of biomass burning combustion sources - burnhut, field, woodstove – high fire and woodstove – start up (delineated by color) re-normalized to the range $-2 \leq logC^* \leq 4$ to enable comparison with the volatility distributions presented in May et al.[2] Distributions are presented in terms of mass fraction in each $logC^*$ bin. The mass fraction showed in each bin is the average bin mass from replicate (N=3) samples while the error bars show the standard deviations in the replicates. The black bars show the distribution from May et al.

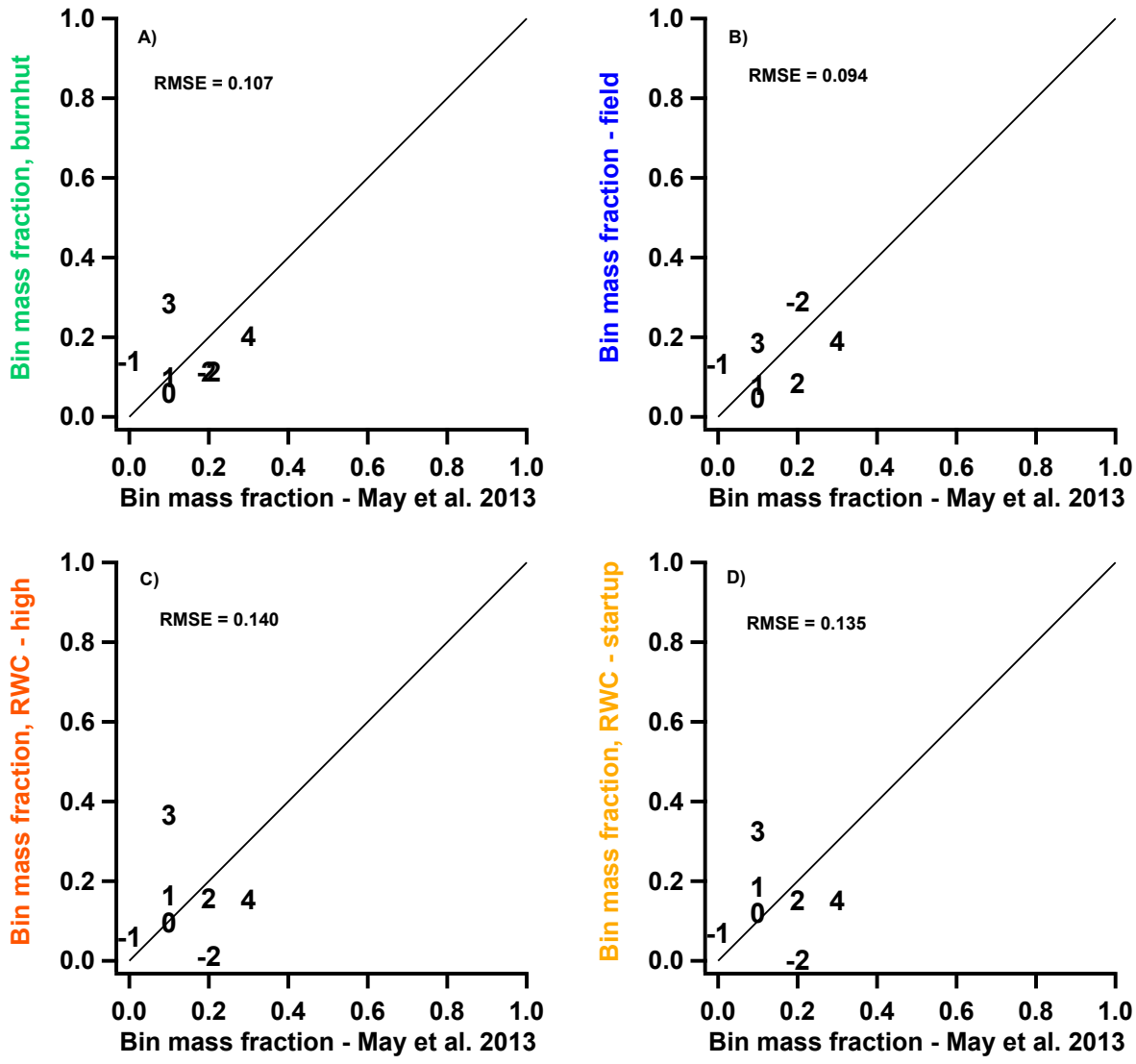

107

108 **Figure S7: Scatter plots of the bin mass fraction contributions from volatility distributions re-**
109 **normalized to the range** $-2 \leq logC^* \leq 4$ **to enable comparison with volatility distributions**
110 **presented in the literature.[2] The plots presented here compare re-normalized burnhut, field, RWC**
111 **– high and RWC – startup distributions to May et al. (delineated by label colors). The markers**
112 **represent the average bin mass fraction from replicate (N=3) filter-in-tube samples. The solid black**
113 **line shows the 1:1 line in each plot with the root mean square error (RMSE) to the 1:1 line printed**
114 **in each plot.**

115

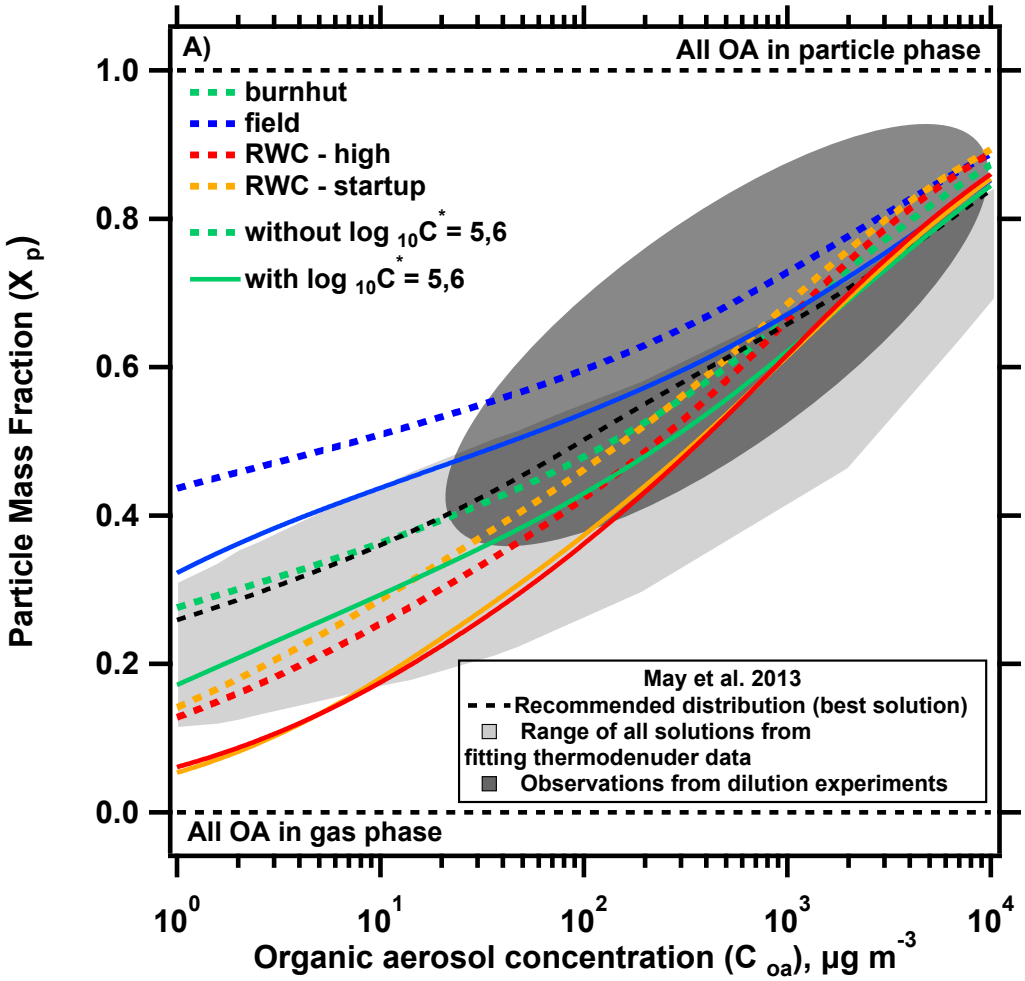

116

117 **Figure S8: Partitioning plot showing the particle mass fraction (X_p) calculated using Equation 1 and**
118 **volatility distributions shown in Figure 3A (containing bins 5 and 6) indicated by the solid and lines**
119 **and Figure S6 (re-normalized after removing bins 5 and 6) indicated by the dashed lines vs organic**
120 **aerosol concentration (C_{OA}). The biomass burning sources are delineated by color. Also plotted are**
121 **observations from May et al.[2] The curves including bins 5 and 6 show the same general trends as**
122 **those using renormalized distributions, but are shifted to lower X_p across the C_{OA} range, as these**
123 **distributions encompass more material. This shift in X_p is less pronounced at higher C_{OA} values as**
124 **more of the IVOC material partitions into the particle phase under these conditions**

125

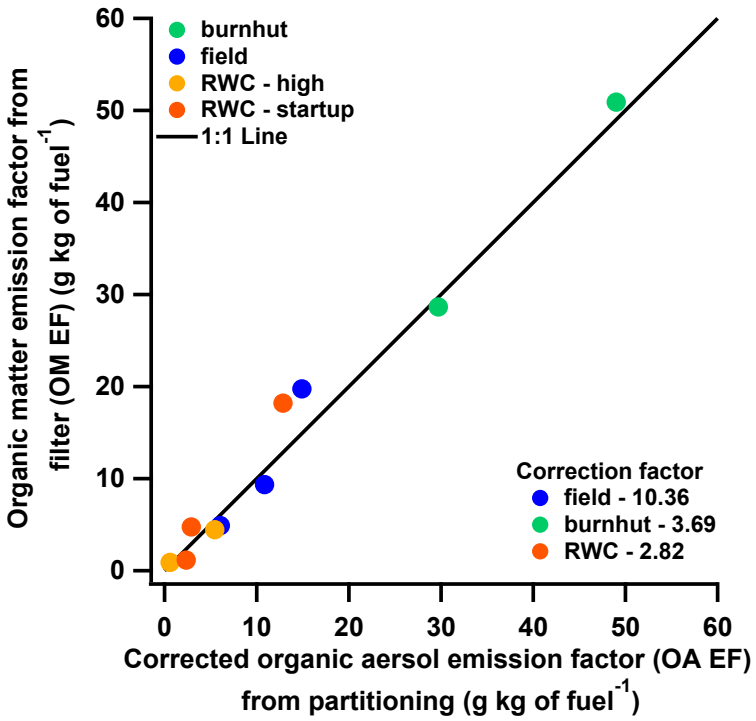

126

127 **Figure S9: Organic matter emission factor (OM EF) as measured via thermooptical analysis of**
128 **quartz filters (converted from OC using a campaign average OM/OC ratio of 1.53) plotted against**
129 **organic aerosol emission factor (OA EF) as estimated from particle phase partitioning of total**
130 **organic matter measured by filter-in-tube filter+sorbents. Colors delineate biomass burning**
131 **combustion source types. The solid black line is the 1:1 line. The correction factors (average of ratio**
132 **for each source type) used to reconcile differences between the two EF estimation methods are**
133 **printed on the graph for each combustion source type.**

134

135 **References**

136 1 E. Grandesso, B. Gullett, A. Touati and D. Tabor, Effect of Moisture, Charge Size, and Chlorine
137 Concentration on PCDD/F Emissions from Simulated Open Burning of Forest Biomass, *Environ. Sci.*
138 *Technol.*, 2011, **45**, 3887–3894.
139 2 A. A. May, E. J. T. Levin, C. J. Hennigan, I. Riipinen, T. Lee, J. L. Collett, J. L. Jimenez, S. M.
140 Kreidenweis and A. L. Robinson, Gas-particle partitioning of primary organic aerosol emissions: 3.
141 Biomass burning, *J. Geophys. Res. Atmospheres*, 2013, **118**, 11327–11338.
142